Petroleum Science 21 (2024) 2037–2047

Contents lists available at ScienceDirect

Petroleum Science

journal homepage: www.keaipublishing.com/en/journals/petroleum-science

Original Paper

Interfacial friction effects on sealing performances of elastomer packer

Peng-Cheng Wang [a], Ming-Hui Chen [b], Jim Jenkinson [a], Yong-Xin Song [c], Li Sun [a, *]

[a] Department of Mechanical Engineering, University of Houston, Houston, TX, 77024, USA
[b] Guren Nanomaterials, Suzhou, 215127, Jiangsu, China
[c] Department of Marine Engineering, Dalian Maritime University, Dalian, 116026, Liaoning, China

ARTICLE INFO

Article history:
Received 23 March 2023
Received in revised form
13 June 2023
Accepted 11 November 2023
Available online 14 November 2023

Edited by Jia-Jia Fei and Min Li

Keywords:
Elastomer seal
Friction
Sealing performance
Contact stress

ABSTRACT

Elastomer sealing performance is of critical importance for downhole tools application including the use of fracturing (Frac) plugs during multi-stage hydraulic fracking. In practice sealing performances of such plugs are normally evaluated through pressure tests, and in numerical simulation studies, maximum contact stress, average contact stress and contact length data are used to determine sealing quality between a packer and casing. In previous studies, the impact of friction forces on sealing performance is often overlooked. This work aims to fill this knowledge gap in determining the influence of friction forces on elastomer packer sealing performances. We first determined the most appropriate constitutive hyperelastic model for the elastomers used in frac plug. Then we compared analytical calculation results with Finite Element Analysis simulation using a simplified tubular geometry and showed the significant influences on interfacial friction on elastomer packer stress distribution, deformation, and contact stress after setting. With the demonstration of validity of FEA method, we conducted systematic numerical simulation studies to show how the interfacial friction coefficients can affect the maximum contact stress, average contact stress, contact stress distribution, and maximum mises stress for an actual packer used in plug products. In addition, we also demonstrated how the groove in a packer can affect packer deformation and evolvement during setting with the consideration of interfacial stress. This study underscores the critical role that friction forces play in Frac plug performance and provides a new dimension for optimizing packer design by controlling interfacial interactions at the packer contact surfaces.

Growing demand for hydrocarbons and depletion of conventional reserve have led to our growing dependence on shale production. Development in shale gas and oil industry has been mainly driven by the advancements in directional drilling and hydraulic fracking technologies, and the effectiveness of multi-stage hydraulic fracturing is contingent upon the performances of frac plugs (Dong et al., 2016; Melikoglu, 2014; Stephenson, 2016). As a mechanical tool that functions to isolate a section of production pipeline to sustain a high fracking pressure, mechanical properties and stress/strain states of the packer determine the performances of the seal. Current frac plugs do not include any sensors and in practice sealing performances of frac plugs can only be evaluated through simple pressure tests. On the other hand, during the design and qualification of frac plugs, specific mechanical criteria have been used to quantify sealing performance and the most commonly used physical parameters are the maximum contact stress, average contact stress, and contact length between the elastomer packer and casing (Patel et al., 2019a, b).

Studies on frac plug sealing performances can be divided into two categories. Large fraction of plug design and optimization studies have focused on investigating packer geometry, design, dimension and material mechanical properties influences on contact and resulted sealing performance. For example, Packer structural design was optimized (Zheng et al., 2021) based on maximum contact stress and deformation displacement data under specific conditions through numerical calculation and experimental validation. Contact stress can be enhanced by increasing the seal radial compression for a tubular structure through expansion or increasing elastomer swelling (Al-Hiddabi et al., 2015). The utilization of a high-pressure sealed preventing shoulder (HPS) design could effectively reduce rubber extrusion and increase contact stress (Dong et al., 2020) and contact stress has a positive

* Corresponding author.
E-mail address: lsun4@uh.edu (L. Sun).

https://doi.org/10.1016/j.petsci.2023.11.015

correlation with Poisson's ratio and a negative correlation with the distance between the rubber packer and the casing surface (Patel et al., 2019a, b). Seals made of AFLAS (Tetrafluoroethylene-propylene) have better sealing performances than HNBR (Hydrogenated acrylonitrile butadiene rubber) in a high-pressure and high-temperature environment (Lan et al., 2019). Groove cross-section shape and size effects on contact stress showed that by placing bearing flow rings in the groove of a packer could effectively improve sealing performance in terms of contact stress (Wang et al., 2017). The sealing performances of packers was evaluated (Hu et al., 2017) using different elastomeric polymers and revealed how material mechanical properties affects sealing performance using contact stress and contact length data. Such studies are mostly numerical.

There are other mechanistic studies uses analytical, numerical and/or experimental approaches but often at the material level or applicable only to much simplified packer geometries. Such studies focus on revealing specific material, temperature, dimension, loading, contact or boundary condition on sealing performances of elastomer products. For examples, researchers conducted analytical studies on how the nonlinear mechanical behavior of elastomer, packer dimension and confinement of packer deformation can affect the sealing performances of a tubular rubber packer (Zhang et al., 2018). The temperature and elastomer stress relaxation effects on the rubber packer was measured and showed that an increase in temperature led to a decrease in both average contact stress and maximum contact stress (Zheng et al., 2021; Zheng and Li, 2021). Numerical as well as experimental studies was implemented to show how the use of guard rings can significantly enhance packer sealing performance when length of the rubber packer falls within a specific range (Chen et al., 2022). Other studies (Evers et al., 2009; Cavalaro and Aguado, 2012) looked at dynamic loading and non-linear material behavior effects the performances of packer products and proposed corresponding design concepts and simulation models.

Despite extensive existing or ongoing research on frac plug mechanics and performance evaluation, little studies have been conducted to quantify the effect of interfacial friction between the packer and casing on sealing performance. Friction force was often neglected or oversimplified in most of studies. Limited research on this topic includes and researchers (Liu et al., 2021; Ma et al., 2014) investigated the friction effect using a 2D FEA model and showed that the contact stress becomes highly nonuniform along the length direction at the packer/casing contact surface, they further concluded that increase in interfacial friction coefficient can reduce sealing performance.

To set a frac plug, axial mechanical loading is required to generate radial expansion in the elastomer packer to make contact with casing. Performance of a frac plug packer refers to its capability of sustaining the pressure differences and preventing liquid leakage during hydraulic fracking operation. As the seal is developed during the plug mechanical setting, the elastomer deformation and stress/strain evolution during this process will dictate its performances. A closer look at how the packer deforms, makes contact with casing and grows the contact area during this setting process tells us that the interfacial friction must affect the stress/strain development and distribution. It is the goal of this research to evaluate and reveal how this often be neglected factor affects the packer sealing performance. Here we report on the investigation of interfacial friction coefficients on the sealing performance of a rubber packer model through a finite element simulation. Simulation was conducted on an actual packer product design which also included central groove and two metal back rings that provide support to the packer at both ends. Here the elastomer is treated as an incompressible material and we found the presence of a groove in the packer structure requires special consideration in numerical simulation to account for boundary conditions when the groove close-up under compression. Our treatment enhances the accuracy of stress analysis in comparison to previous studies, which ignored the changes and disappearance of groove surfaces. This research provides a comprehensive approach and analysis for frac plug design and optimization.

1. Model setup

1.1. Frac plug structure and its working principle

Fig. 1(a1) shows the schematic cross section structure of a horizontal well with two fracked sections and one perforated but not yet fracked section. The primary function of the frac plug is to isolate the perforated section from the fractured sections so that the fracking fluids pumped down from surface can be maintain at high pressure level to fracture shale formation through the perforated holes with as little as possible fluid leak to the perforated sections. In accomplishing its function, traditional frac plug design includes following critical components: lower slip, lower cone, elastomer packer, upper cone, upper slip, and mandrel (Fig. 1(a2)). To provide mechanical support and confine elastomer extrusion under axial compression, support rings with matching geometry and dimension are often used at the two ends of the packer (as

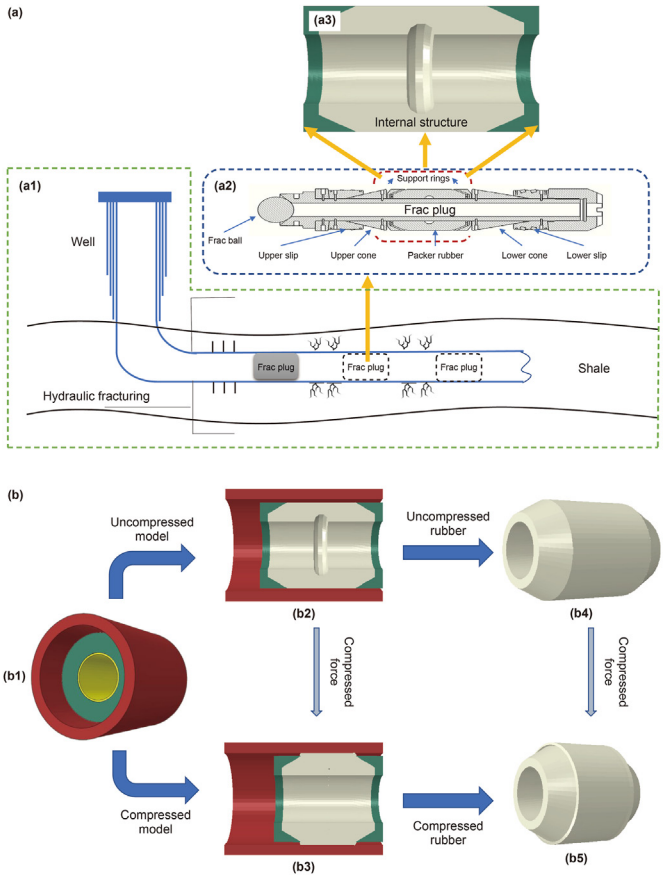

Fig. 1. (**a**) Schematics of the cross sections of (**a1**) a partially completed well (**a2**) frac plug with a frac ball and (**a3**) a packer with support rings before setting. (**b**) Schematic drawings of the sealing section of a frac plug before and after activation (**b1**) physical model used in numerical simulation, (**b2**) cross section of the model before plug setting, (**b3**) cross section of the model after plug setting, (**b4**) 3D model of the elastomer packer before setting and (**b5**) 3D model of the elastomer packer before after setting.

shown in Fig. 1(a3)). After delivering the assembled plug to the desired location, the setting tool will be activated to so that a large enough compression will be applied along the plug axial direction to first expand the slips radially and anchor the plug to the internal casing surface, in the meanwhile, the compressive force upon the elastomer packer along the longitudinal direction will introduce radial expansion and result in a sealing contact between the packer out surface and casing internal surface. Fig. 1(b) shows the schematics of the sealing section of the frac plug before and after activation which includes the packer, casing, support rings, and mandrel as the main components for this study.

1.2. Physical model setup

Fig. 2 shows the detailed 3D physical model constructed for the sealing section of the frac plug together with production casing. Four components are included in the model: elastomer packer, casing, two support rings and mandrel. Critical dimensionality parameters specified the shape and size and geometric correlations of these components used in our study are summarized in Table 1. Here we assume mandrel diameter equals the internal diameter of the elastomer packer. Also included in the model is a groove with half-circle cross section located in the middle of the packer. Friction forces can develop between the packer internal surface and mandrel (f_1) and the packer external surface and casing (f_2). According to Fig. 2 configuration, during setting of frac plug compressive forces are applied along the structure axial direction (x-direction) and right surface of support ring is fixed.

1.3. Elastomer mechanical constitutive modeling determination

Elastomers often exhibit highly nonlinear elastic behavior, especially under significant loading conditions. For packer sealing performance evaluation under high pressure, it is necessary to choose appropriate constitutive model that can account for the non-linearity of the mechanical responses of elastomeric material in improving finite element analysis accuracy. Also in FEA modeling, it is also crucial to ensure convergence of numerical calculation (Bergstrom and Boyce, 1998). Considering the nonlinear, incompressible and isotropic characteristics of the hyperelastisity, various constitutive models, Non-Hookean, Mooney-Rivlin, Ogden, and Yeoh (Kim et al., 2012) have been developed to quantify the hyperelastic mechanical behavior of elastomers based on train energy analyses. It is essential to choose the most appropriate constitutive model for the elastomer used for packer production so that more reliable and accurate numerical calculations can be conducted. In this study we used the experimentally measured

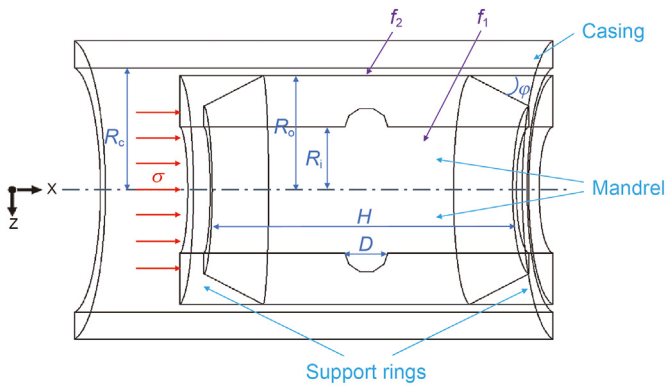

Fig. 2. Schematic diagram of the physical model.

Table 1
Parameters used for simulations.

Components	Symbol	Value	Unit
Length of rubber	H	136	mm
Internal radius of packer rubber	R_i	29.5	mm
External radius of packer rubber	R_o	53.5	mm
Internal radius of casing	R_c	57.15	mm
Groove diameter	D	18	mm
Contact angle	φ	30	°

tensile and compression stress-strain data to determine the most suitable constitutive model use in further FEA simulation.

Generally, the Non-Hooken model (Ogden, 1997) is only applicable to the initial part of smaller elastomer deformation since it only includes a linear constant when calculating the strain energy as:

$$W = C_1(I_1 - 3) \tag{1a}$$

where C_1 is a material constant, and I_1 is the first invariant of the left Cauchy-Green deformation tensor.

The Mooney–Rivlin model (Mooney, 1940; Rivlin and Saunders, 1997) calculates the strain energy density function using a linear combination of the two invariants of the left Cauchy-Green deformation tensor, and for an incompressible elastomer it can be written as:

$$W = C_{10}(I_1 - 3) + C_{01}(I_2 - 3) \tag{2a}$$

where C_{10} and C_{01} are material constants and I_1 and I_2 are the first and second invariants of the deviatoric component of the left Cauchy-Green deformation tensor. This model extended the applicable strain range to medium strains, typically up to 100% for tensile strain and 30% for compressive strain.

Then the Odgen model (Ogden, 1972) was established on including the principal stretches of the left Cauchy-Green strain tensor, rendering it being compatible with various hyperelastic constitutive relationships. In this model, the strain energy density function has the following expression:

$$W = \sum_{i=1}^{N} \frac{\mu_i}{\alpha_i}\left(\lambda_1^{\alpha_i} + \lambda_2^{\alpha_i} + \lambda_2^{\alpha_i} - 3\right) + \sum_{k=0}^{n} \frac{1}{D_k}(J-1)^{2k} \tag{3a}$$

where N is the order of the model. Theoretically when including all high order terms, this model can account for the material elastic mechanical behavior across the entire strain range, and exhibits non-uniform shear modulus and with limited amount of compressibility. In practice, $N = 3$ is the most widely used and for this Odgen-N3 model, μ_i and α_i are the materials constant, where μ_i has the unit of pressure and α_i is a dimensionless factor. D_k is an incompressible parameter and $J = 1$ when the material is incompressible.

Finally, the Yeoh Model (Yeoh, 1993) added an exponentially decaying term to the strain energy density function as:

$$W = \sum_{i=1}^{N} C_{i0}(I_1 - 3)^i + \sum_{k=1}^{N} \frac{1}{D_k}(J-1)^{2k} \tag{4a}$$

where J is the volume ratio and for incompressible materials, $J = 1$, I_1 is the first invariant of the Cauchy-Green strain tensor. The Yeoh model does not consider the second invariant I_2 as in the Mooney-Rivlin model. However, the volumetric terms of Yeoh are more complex than those of Mooney-Rivlin model. When $N = 1$, Yeoh is equivalent to the Neo-Hookean model. The Yeoh model only needs

a few data points to provide reasonable fitting results and the input data can be just coming from a uniaxial tensile test. This model tends to loose accuracy when predicting biaxial and other complex deformations.

In this study we use uniaxial tensile and compression test data as shown in Fig. 3(a) and (b) to test against the above mentioned four constitutive models. Only the Non-Hookean and Ogden-N3 models can yield stable output (Table 2), and when comparing the uniaxial tensile stress-strain results, the Ogden-N3 model generated data closest to the experiment measurements for strain exceeding 300%. Thus, the Ogden-N3 model is used in subsequent FEA modeling shown in Fig. 4.

1.4. Analytical mechanical analysis on a tubular structure

For a tubular rubber packer, it is possible to carry out analytical stress/strain analyses in the elastomer with certain simplified boundary conditions and geometric confinements. Mechanical analyses were conducted (Liu et al., 2014) on such a tubular packer deformation during the mechanical setting process. As illustrated in Fig. 5, the packer deformation evolves across four stages. In the cylindrical coordinates, the thick wall cylinder mechanical analyses provide the following stress equations (Crossland et al., 1959; Júnior et al., 2023).

$$\sigma_r = \frac{r_i^2 p_i - r_o^2 p_o}{r_o^2 - r_i^2} - \frac{(p_i - p_o) r_i^2 r_o^2}{(r_o^2 - r_i^2) r^2} \tag{1b}$$

$$\sigma_\theta = \frac{r_i^2 p_i - r_o^2 p_o}{r_o^2 - r_i^2} + \frac{(p_i - p_o) r_i^2 r_o^2}{(r_o^2 - r_i^2) r^2} \tag{2b}$$

where σ_r is the radial stress, σ_θ is the hoop stress, σ_z is the axial stress, p_i is the internal pressure, p_o is the external pressure, r_i is the internal radius, r_o is the external radius, r is the radius at the point between r_i and r_o.

Liu et al. (2021) included friction forces at the inner and out packer surfaces and established the axial direction (z-axis) stress balance equation as:

$$\sigma_z = \frac{F_1 + F_2 - F_z}{\pi(r_o^2 - r_i^2)} \tag{3b}$$

Here F_1 is the friction force between the mandrel and the internal rubber packer surface, and F_2 is the friction force between the casing and the external rubber packer surface, F_z is the sealing force. These two terms of friction forces are determined by the product size of contact area and the friction per unit area as:

$$F_1 = 2\pi r_i Z_\Delta f_1 p_i \tag{4b}$$

$$F_2 = 2\pi r_o Z_\Delta f_2 p_o \tag{5}$$

where f_1, f_2 are the friction coefficients the packer and mandrel interface and at the packer and casing interface, respectively; Z_Δ is the contact length of the interfaces and p_i and p_o are the contact stress at the respective interfaces.

Now assume the contact stresses of the two interfaces are equal $p_i = p_o$ and in the final compressed state, both internal and external surfaces of the rubber packer make full contact with the mandrel and casing, the relationship between contact stress and axially applied setting force can be derived as:

$$p_o = \mu F_z / [2\pi\mu Z_\Delta (r_i f_{1+} r_o f_2) + \pi(1-\mu)\left(r_o^2 - r_i^2\right)] \tag{6}$$

In this analytical analysis, the contact stress calculation is based on force balance and it is assumed after the setting the packer deformation is uniform throughout the entire packer. As shown in Fig. 5, in this calculation the external surface of the packer makes full contact with casing and the pressure and resulted friction force are considered to be the same along the longitudinal direction of the contact surfaces. During actual application, the contact length depends on the applied setting force and the stress/strain distribution in the packer, as well as the interfacial contact stress and friction distribution along contact length are nonuniform. Also, the effects of the existence of the gaps between the support ring and

Table 2
Stability of four constitutive models when used to fit mechanical responses of the elastomeric packer material.

Loading method	Neo-Hooken	Mooney-Rivlin	Odgen-N3	Yeoh
Uniaxial tension	Stable	Unstable	Stable	Unstable
Uniaxial compression	Stable	Unstable	Stable	Unstable
Biaxial tension	Stable	Unstable	Stable	Unstable
Biaxial compression	Stable	Unstable	Stable	Unstable
Planar tension	Stable	Unstable	Stable	Unstable
Planar compression	Stable	Unstable	Stable	Unstable

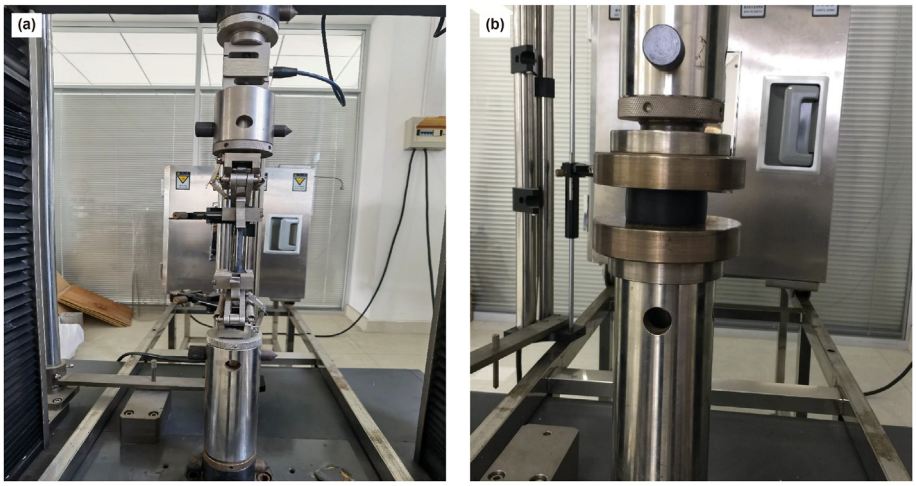

Fig. 3. Pictures of the experimental setup of (**a**) uniaxial tensile and (**b**) uniaxial compression tests of the elastomer samples.

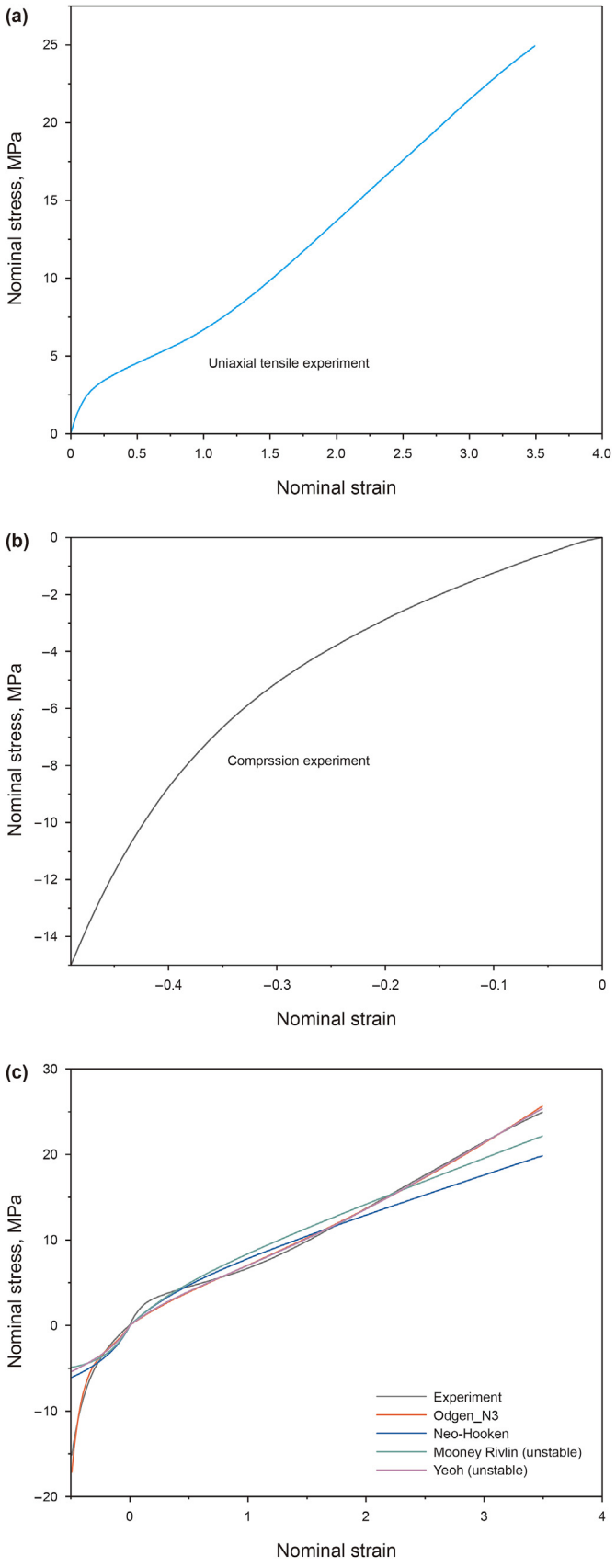

Fig. 4. Stress-strain curves of (**a**) uniaxial tensile measurement, (**b**) uniaxial compression measurement and (**c**) fit results obtained from the four constitutive models and the uniaxial tensile measurement.

case are difficult to account for in such analytic modeling. But such analysis provides quantitative baseline estimation that can be used as reference data.

1.5. FEA simulation procedures

In this study, the materials used for different components and their mechanical properties are listed in Table 3. All components other than the packer are considered to have linear elastic behavior, and Odgen-N3 model is applied to the packer. Finite element analysis was carried out in ABAQUS.

FEA analyses have been applied to two packer geometries, first is for the tubular geometry and then for an actual packer used in frac plugs with more complicated geometry. For tubular packer modeling, standard linear element C3D8R were used to mesh the casing section and the two support rings and the rubber packer was meshed using the hybrid formulation element C3D8RH. As shown in Fig. 6(a) to (c), there were a total of 13,704 linear hexahedral C3D8R elements and 16,694 C3D8RH elements used.

Fig. 6(d)–(f) show the geometry of actual elastomer packer, supporting rings and mandrel, together with the meshing schematics, and loading/boundary condition setup. 13,794 C3D8RH elements were used to mesh the rubber packer and a total of 19,637 C3D8R elements used to mesh other parts. Because the actual packer contains two tapering ends and a groove, the determination of how to mesh the packer and number of elements are decided after careful balancing of accuracy and computation efficiency. We compared the simulated results from using 6466, 13794 and 26076 C3D8RH elements, and differences from using these three element numbers are within 3%.

2. Results and discussion

2.1. Comparison between analytic modeling and FEA results for the tubular elastomer geometry

In our FEA simulation, a 25 MPa setting stress was applied from one end of the packer through support ring and the bottom surface of the opposite ring is fixed. In following presented results, the packer and casing are oriented vertically, with bottom support ring surface fixed and the setting stress is applied to the top support ring downwards. Fig. 7(a) summarizes the FEA calculated contact stress distribution along the tubular rubber axial direction with different interfacial friction coefficients (assuming $f_1 = f_2$). From the top loading surface contact stress follows a general trend of decreasing when moving along towards the bottom fixed plane, contact stress abnormality at the two ending regions are resulted from gap between the support ring and casing where local elastomer extrusion can be taken place. After the setting load is applied, deformation of the elastomer packer went through a dynamic process and the generation of interfacial friction affects the stress/strain development and distribution in the packer and at contacting interfaces. Before setting, the elastomer packer is assumed to only make zero stress contact with support ring and mandrel. Dynamic friction forces will be generated only after packer makes nonzero stress contact with the casing and the mandrel and when there is relative sliding at the interfaces. Generated dynamic friction force is in the opposite direction to the applied load direction and this counter effects accumulates from the top where there is more significant vertical packer displacement. As the magnitude of the friction force can be estimated by the product of contact stress (normal to interface), contact area and friction coefficient. With increasing friction coefficient and same other parameters, there is faster drop in contact pressure along the longitudinal direction of the packer. In

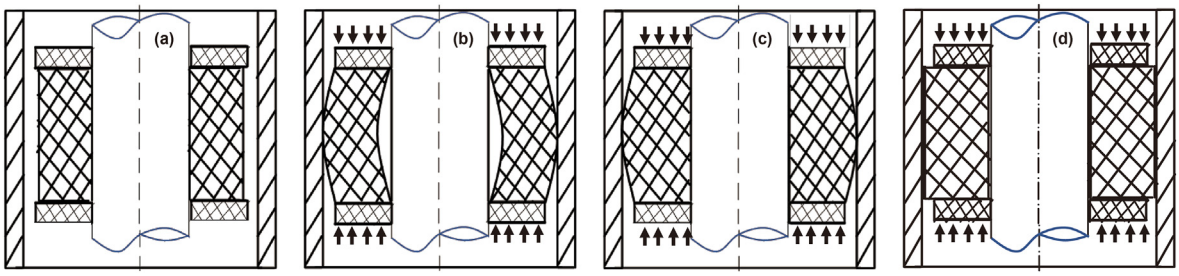

Fig. 5. The deformation of the rubber packer.

Table 3
Material parameters of the frac plug.

Components	Material	Elastic modulus, MPa	Poisson's ratio
Casing	35CrMo steel	209000	0.28
Packer rubber	Rubber	Nonlinear	0.49
Support rings	Mg–Al alloy	49000	0.29
Mandrel	40CrNiMoA	209000	0.28

other words, interfacial friction will reduce the effect of externally applied setting stress.

A comparison of the interfacial friction effects on the average contact stress obtained from FEA modeling and analytical calculation using Eq. (6) is shown in Fig. 7(b) (Same setting stress of 25 MPa). Both curves have the same trend of decreasing in contact stresses with increasing friction coefficient. Average contact stress value obtained from FEA are lower than the corresponding values calculated from analytical model. In analytical modeling, the support ring-casing effect is neglected and the packer deformation along the axial and radial directions are assumed to be uniform throughout the elastomer tube. Such geometric confinement and assumptions can result in an overestimation in stress. In addition,

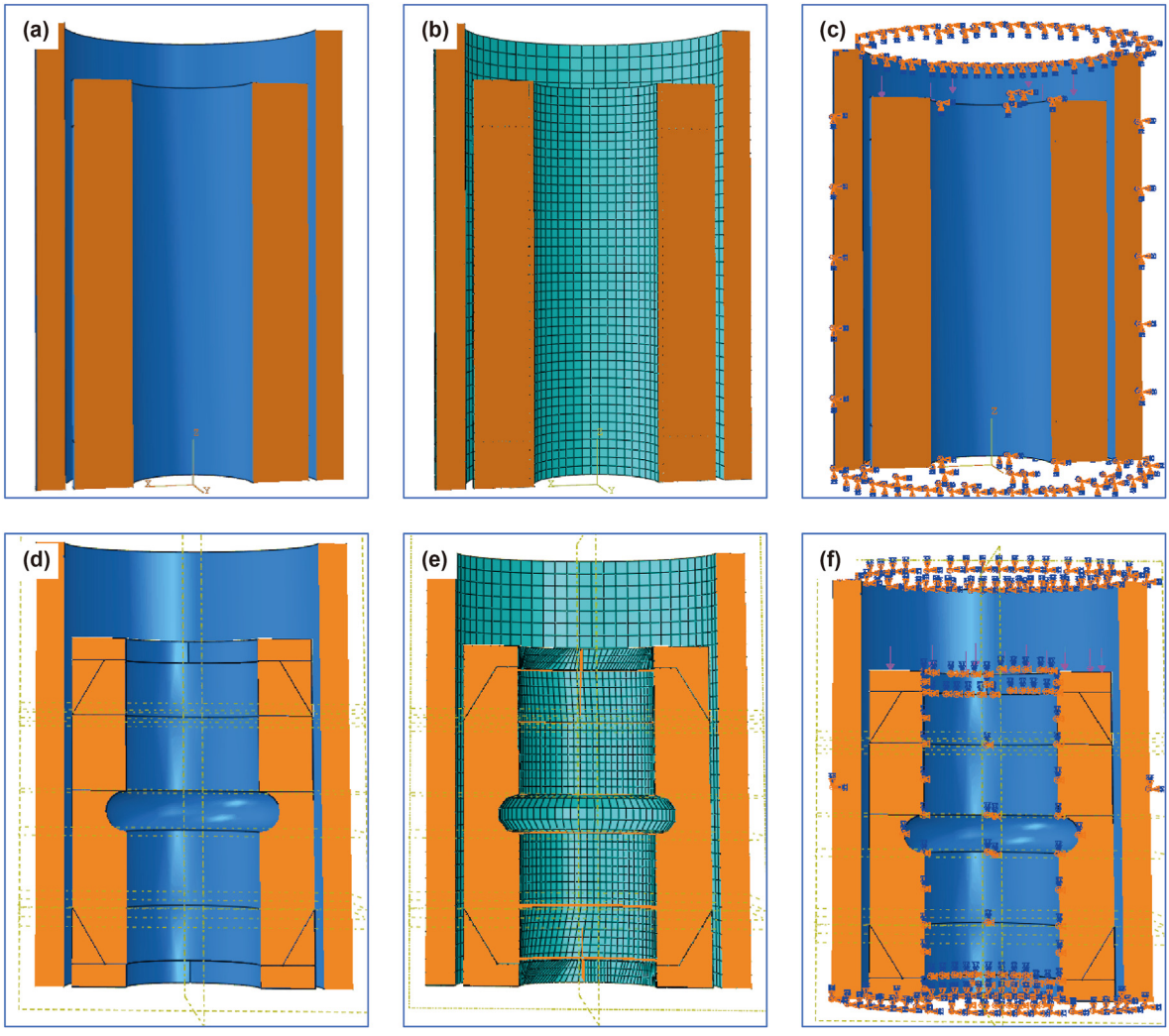

Fig. 6. Numerical simulation setup for the simplified tubular packer geometry (**a**–**c**) and actual packer and plug components (**d**–**f**).

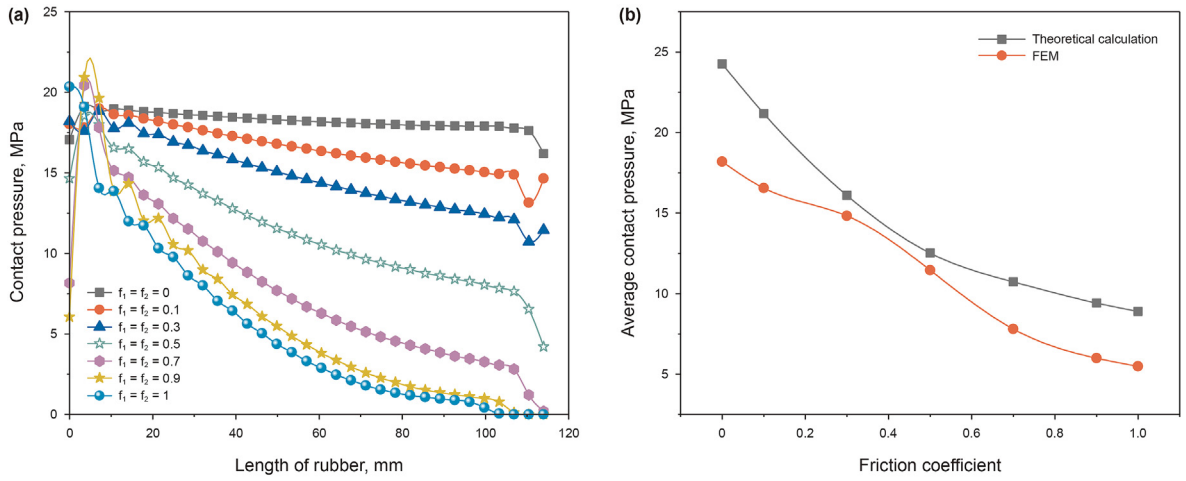

Fig. 7. (**a**) FEA calculated contact stress distribution the length direction at the packer-casing/mandrel interface along with different interfacial friction coefficient. (**b**) Comparison of the average contact stress obtained from analytical model and FEA dependences on interfacial friction coefficient.

the analytic modeling directly applied the product of contact stress, contact area and friction coefficient as the friction force to the force balance equation, this is problematic since in the packer will be in a stabilized static state and there should be zero dynamic friction force. It is possible in this state, there exists static friction, but the force balance analyses should take into account other forces provided by the supporting components of the frac plug.

2.2. Numerical simulation results for actual packer geometries

2.2.1. Interfacial friction effects on packer/casing interface contact stress development

Dimensionality data for FEA modeling of an actual elastomer packer are listed in Table 1. When a frac plug is activated and set under the externally applied mechanical loading, friction will be generated at the packer/casing (external) and packer/mandrel (internal) two interfaces. Interfacial dynamic friction is determined by a serial of factors such as material, surface roughness, temperature, loadings, relative speed of motion etc. Here a direct proportional relationship between friction force and contact stress, characterized by the friction coefficient f, is used in this study. We first studied the effects of external and internal friction forces on interface contact stress. Fig. 8 shows four sets of simulation results when considering the internal interface friction coefficient f_1 is (a) frictionless = 0, (b) = 0.3, (c) = 0.7 and (d) = 1.0 while varying the external interface friction coefficient f_2 between 0 and 1.0.

Under current loading condition and configuration, it is found that the packer makes full contact with casing in all 16 simulations and maximum contact stress appears along gap area formed top support ring and casing, elastomer extrusion can be clearly identified in this region with high level of stress concentration. Fig. 8(a1) shows the contact stress distribution when $f_1 = f_2 = 0$, which is the friction free state or when the friction effect was neglected as in most of previous studies. Without interfacial friction, contact stress has a uniform distribution along the length direction of the contact, except for locations near the contacts with the supporting rings and corresponding to the groove position. It is clear from comparisons with the rest of the simulation results that interfacial friction, both at the internal and external surfaces will significantly affect the stress/strain distribution in elastomer packer and further influences its sealing performances.

A comparison of Fig. 8(a1), (b1), (c1) and (d1) shows that while keeping the external interface friction free, the contact stress tends to accumulate more significantly towards the top portion of the packer with an increase in internal friction coefficient. This can be attributed to the fact that the friction at the external interface develops from top-down and the friction force direction is opposite to the loading force direction, and the larger the internal friction coefficient the more significant the stress concentration effect. This contact stress concentration effect is less prominent for the external interface friction force; as shown in Fig. 8(a1), (a2), (a3) and (a4) when the internal interface maintains as friction free, with increasing external interface friction interface, there is also contact stress redistribution and concentrating effect at the top portion of packer but at a lower extent. We attribute such effects to the different boundary confinement at the packer/casing contact near the support ring and at the packer/mandrel interface, where elastomer relaxation through extrusion can occur in the previous case.

To better quantify the interfacial friction forces effect, in Fig. 9 the FEA calculated contact stress along the length of the packer/casing contact length were plotted, as grouped by the f_1 and f_2 inputs. For all cases, with and without interfacial friction, maximum contact stress occurs in the region close to the loading surface and top-support ring and casing gap. The bottom support ring and casing gap area always has the lowest contact stress. This is consistent with observation that elastomer failure always happens at one end of the packer around contact surface. It is also true that the contact stress has higher value in the middle part of the packer, which directly reflects the effect of including grooves in the packer design (details will be discussed in the following section).

Excluding the stress concentration effect introduced by the groove, the FEA simulation results show the clear effects of interfacial friction on contact stress values and distribution. Non-zero interfacial friction will result in stress concentration from the top surface. Under any fixed internal friction coefficient (f_1 is constant), increase in external friction coefficient f_2 will result in reduction of local contact stress, and reduction rate along the length of the contact surface also increases. Such effects are more prominent for small f_2 and under current simulation conditions, such effects diminish when f_2 is larger than 0.3, regardless of value of f_1. In comparison, when external friction coefficient f_2 is held at constant, increases in f_1 will not result in significant change in the shape of the contact stress distribution curve, but the value of local contact stress has significant continuous reduction in the entire studied range of 0–1.

Fig. 10 uses the 3D contour plot to show how the calculated maximum contact stress at the packer-casing interface depends on the two interfacial friction coefficients f_1 and f_2. A maximum

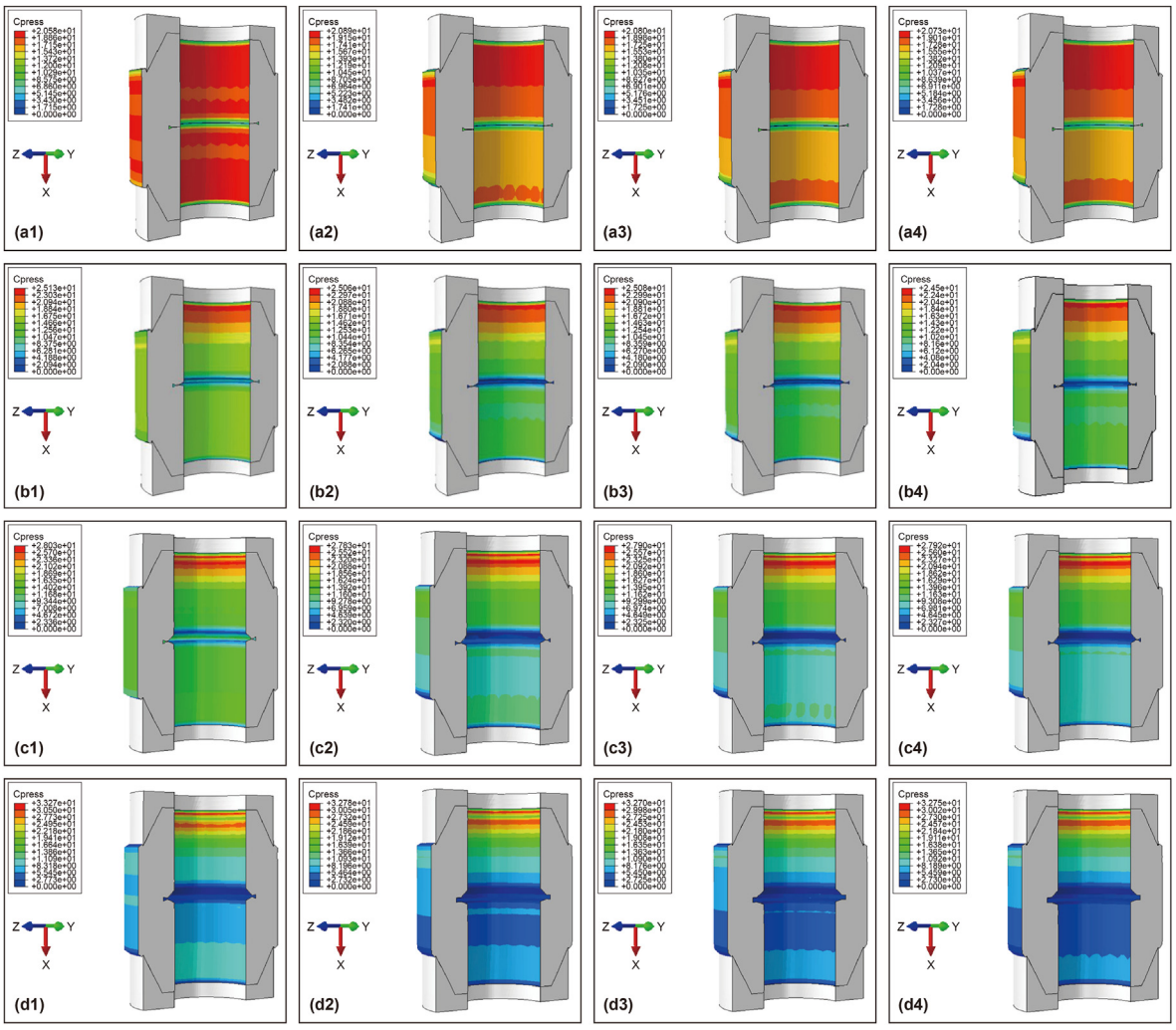

Fig. 8. FEA calculated contact stress distribution after the elastomer packer set with 25 MPa load with diffident internal (packer/mandrel) and external (packer/casing) surface friction coefficients configurations (f_1 and f_2). Serial (**a**) $f_1 = 0.0$; Serial (**b**) $f_1 = 0.3$; Serial (**c**) $f_1 = 0.7$ and Serial (**d**) $f_1 = 1.0$. For each serial, four values of f_2: 0.0, 0.3, 0.7 and 1.0 were considered.

contact stress value of 21.7 MPa for frictionless interfaces is more than twice the value of minimum contact stress of 9.3 MPa when external interface is frictionless and internal surface has the largest calculated friction coefficient of $f_1 = 1$. This plot also provides direct visualization that the changes in f_1 has more significant impact on the maximum contact stress than the changes in f_2.

This part of study clear demonstrates the non-negligible effects of interfacial friction on the stress/strain development in elastomer packer. Packer/casing contact stress has a nonlinear distribution along the length of packer, gap between the support ring and groove in the packer can affect the local contact stress distribution. Interfacial friction on the other hand can have significant impact on the global contact stress distribution.

2.2.2. Groove effect

In most of the packer design and products there is a groove in the middle of the internal surface. When axial compressive loading is applied, such as in the frac plug setting process, this groove will promote bulging deformation from the middle of the packer. As being demonstrated in Figs. 8 and 9, groove in the packer will trigger the stress concentration effect and bulging of the packer will introduce a contact and sealing process that can be described in Fig. 5. For a packer with uniform tubular geometry and no groove, previous FEA results presented in Fig. 7(a) show that there is stress concentration effect in the top support ring-casing gap area, and along the axial direction, contact stress decreases monotonically when moving towards the bottom fixed surface. Under such circumstances, packer-casing contact will be initiated in the gap region and elastomer failure will also be initiated from such high stress concentration region. Utilization of the groove for stress redistribution and initiation of local deformation and contact of packer with casing can be well justified from current FEA simulation results. As the current study focus on quantify of the interfacial friction effects, the effect of groove size, cross section geometry and location will not be discussed here. For the groove size and other geometrical and material parameters fixed (listed in Tables 1 and 3), FEA results show that the stress concentration effect is most prominent when $f_1 = f_2 = 0$, and the effect diminishes with increasing friction coefficient.

2.2.3. Interfacial friction effects on the maximum mises stress in packer

As the interfacial contact between packer and casing directly determines the sealing performances of frac plug, it is also important to know the stress/strain distribution in parker which dictates the elastomer material and the stability of the packer during

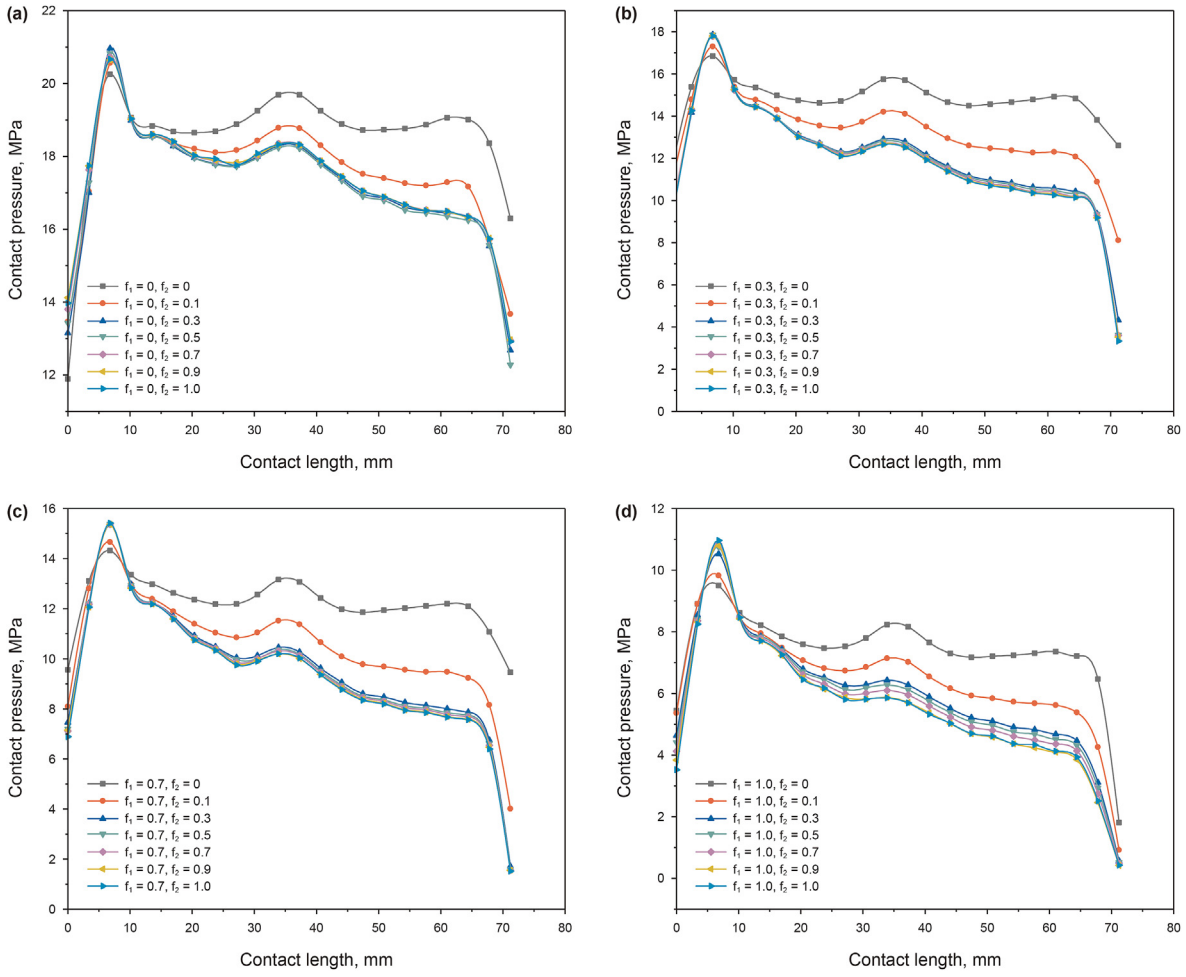

Fig. 9. FEA calculated contact stress distribution along the axial direction of the packer/casing contact for different internal and external interfacial friction coefficients. (**a**) $f_1 = 0.0$ with varying f_2; (**b**) $f_1 = 0.3$, with varying f_2; (**c**) $f_1 = 0.7$ with varying, and (**d**) $f_1 = 1.0$ with varying. f_2.

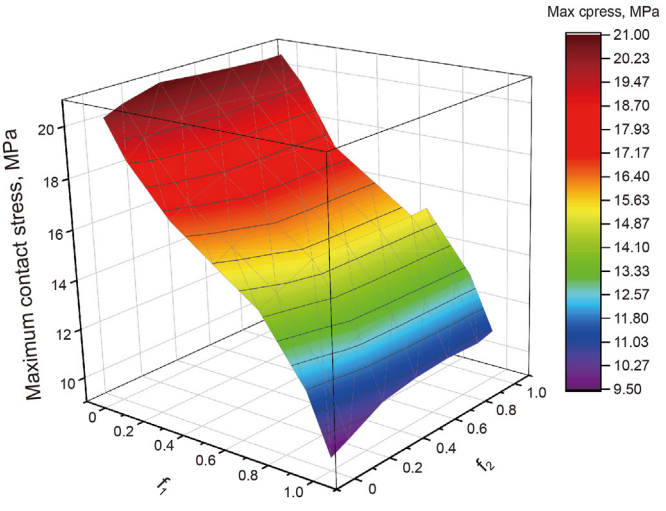

Fig. 10. Maximum packer-casing contact stress dependences on the internal and external interfacial friction coefficients f_1 and f_2.

operation. Fig. 11 shows the FEA calculated Von Mises stress for four sets of f_1: (a) frictionless = 0, (b) = 0.3, (c) = 0.7 and (d) = 1.0 while varying the external interface friction coefficient f_2 between 0 and 1.0. When compared to the corresponding interfacial contact stress distribution has been discussed earlier, there are similarity as well as differences. It is also very clear that interfacial friction and groove as well as the gap between the support ring/casing have non-negligible impacts on body Mises stress distribution in the packer. While the groove and gap will both result localized stress non-uniformity, friction at the contact surface can significantly modulate the global stress distribution. Elastomer extrusion from the top support ring-casing gap can be observed in all simulated cases and such area is not the largest Von Mises stress area, this is very different from the contact stress distribution. With zero internal friction coefficient (f_1), there is Mises stress concentration effect in the surrounding area of the groove tip, regardless of the value of f_2. As shown in Fig. 11(a1–a4) increase in f_2 will introduce more significant stress concentration towards the top surface, but the largest Von Mises stress remains in the groove area, because when internal interface is frictionless, the groove opening will have larger deformation which will result in higher stress concentration effect.

Now look at the internal friction effect on Mises stress with fixed f_2. A comparison among Fig. 11(a1), (b1), (c1) and (d1) showed that while the external interface remains friction free, increasing in internal friction coefficient (f_1) will reduce the groove stress concentration area and shift the highest Mises stress area towards the top contact region of packer and mandrel. This is because internal interface friction will limit groove deformation and the smaller

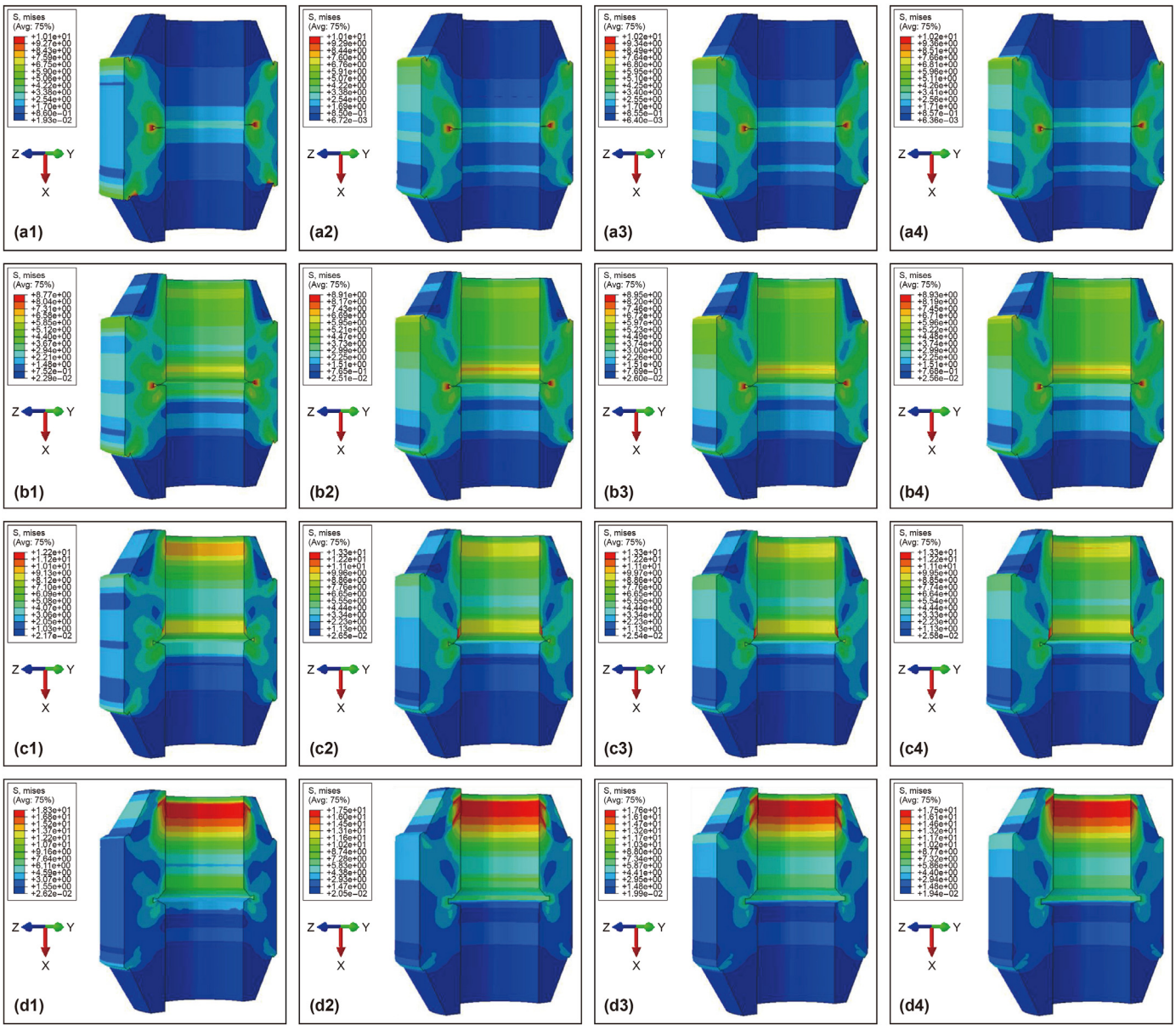

Fig. 11. FEA calculated Mises stress distribution after the elastomer packer set with a 25 MPa load with diffident internal (packer/mandrel) and external (packer/casing) surface friction coefficients configurations (f_1 and f_2). Serial (**a**) $f_1 = 0.0$; Serial (**b**) $f_1 = 0.3$; Serial (**c**) $f_1 = 0.7$ and Serial (**d**) $f_1 = 1.0$. For each serial, four values of f_2: 0.0, 0.3, 0.7 and 1.0 were considered.

groove compressive deformation, the lower the stress concentrate effect in surrounding area. In the meanwhile, larger f_1 will also result in larger friction forces for the same contact stress, which can be reflected in higher confrontation effect of the Mises stress. For all 16 FEA simulated cases, the largest Mises stress with a value of 18.3 MPa appears when $f_1 = 1.0$ and $f_2 = 0.0$, in the top contact region of the packer with support ring and mandrel. In comparison, when $f_1 = f_2 = 0$, a maximum Mises stress value of 10.1 MPa can be found in vicinity of the groove. This study again demonstrates the significant effects of interfacial friction on mechanical states of the packer and the need to include the frictions at both interfaces in packer design and application.

3. Conclusions

Elastomer sealing performance is of critical importance for applications in oil/gas, chemical and aerospace industries where operation conditions are extremely harsh and safety consequences are significant. Packers used in hydraulic fracturing plug products are expected to sustain a 70 MPa pressure difference, keep sealed at various downhole temperatures (from 50 to 180 °C and above), and survive complicated chemical and flow conditions. Such applications not only challenge elastomer intrinsic physio-chemical property limits but the packer performances are also affected by the complex geometry/contacts, large sizes, and various static/dynamic loading conditions. While application requirements push the material limits and challenge product design, often times the stress/strain in the sealing element are very difficult if not impossible to determine and largely remains unknown. In practice, the sealing performance of elastomer components is simply evaluated through pressure tests, and design modifications/optimizations are mostly conducted based on empirical analyses. Sealing performance criteria are not well established, and the dynamic seal setting process and consequent stress/strain evolution are not well

understood. Here we report on the development of finite element modeling for stress/strain analysis of elastomer packers after mechanical setting. We first compared the experimentally measured uniaxial tensile stress-strain curve of the packer elastomer with data generated by different super-elasticity constitutive models to choose the model with generated results fit best with measurement. The chosen Ogden-N3 model was adopted for all following FEA simulation. For a tubular packer geometry, FEA simulation clear shows that increase in interfacial friction force will result in a faster drop in packer/casing contact stress from the loading surface and towards the fixed surface; average contact stress over the contact length also decreases with increasing friction coefficient. Such trend fits well with the analytic correlations derived from force balances with simplified boundary conditions. Based on this, we then conducted systematic FEA simulation for an actual packer with matching support rings with a setting pressure of 25 MPa. The effects of interfacial friction on the interfacial contact stress (which determines sealing performances of the frac plug) and body Mises stress (which determines the frac plug safety and stability) in the packer were carefully examined. Elastomer can be extruded out from the gap formed by the top support ring and the casing, resulting in increases in contact stress and decreases in Mises stress. An inside groove at the middle plane of the packer creates a local Mises stress concentration effect which enables the initiation of bulging deformation in packer and enables the formation of a more stable seal. Highest contact stress can be found in the gap area when both internal (packer-mandrel) and the external (packer-casing) interfaces are frictionless. Increase in interfacial friction can effectively lower average contact stress and create larger contact stress difference between the load and fixed end. Similar concentration effect in Mises stress has also been observed when varying the two friction coefficients, and the groove deformation and local Mises stress concentration are very sensitive to the internal friction force. While increase in contact stress and packer contact length will improve the sealing performance through by reducing liquid permeation under large pressure differences. Friction force at the two interfaces should be taken into consideration during frac plug design and application. Both can significantly affect the maximum, average and distribution of the contact stress and Mises stress. Such effects will be different for different component design, casing sizes, and setting conditions. The capability of modifying the interfacial friction coefficient through physical or chemical treatment will be worthwhile in improving sealing performances. This study focuses on the revelation and treatment of interfacial friction in determining packer mechanical performances. There are many other geometric, materials, operational parameters will also affect the sealing performances. Future studies combine numerical modeling, experiment measurement and machine learning can provide further insight into the design and optimization of hydraulic fracking plugs.

Declaration of competing interest

The authors declare that they have no known competing financial interests or personal relationships that could have appeared to influence the work reported in this paper.

References

Al-Hiddabi, S.A., Pervez, T., Qamar, S.Z., et al., 2015. Analytical model of elastomer seal performance in oil wells. Appl. Math. Model. 39 (10–11), 2836–2848. https://doi.org/10.1016/j.apm.2014.10.028.

Bergstrom, J.S., Boyce, M.C., 1998. Constitutive modeling of the large strain time-dependent behavior of elastomers. J. Mech. Phys. Solid. 46 (5), 931–954. https://doi.org/10.1016/S0022-5096(97)00075-6.

Cavalaro, S.H.P., Aguado, A., 2012. Packer behavior under simple and coupled stresses. Tunn. Undergr. Space Technol. 28, 159–173. https://doi.org/10.1016/j.tust.2011.10.008.

Chen, Y., Liu, X., Li, C., 2022. Development of rubber packing element for 105 MPa/215 °C deep-well test packer. Materials 15 (6), 65–74. https://doi.org/10.3390/ma15062024.

Crossland, B., Jorgensen, S.M., Bones, J.A., 1959. The strength of thick-walled cylinders. J. Eng. Ind. 81 (2), 95–111. https://doi.org/10.1115/1.4008259.

Dong, D., Wang, Y., Li, X., et al., 2016. Breakthrough and prospect of shale gas exploration and development in China. Nat. Gas. Ind. B 3 (1), 12–26. https://doi.org/10.1016/j.ngib.2016.02.002.

Dong, L., Li, K., Li, B., et al., 2020. Study in deep shale gas well to prevent shoulder protruding packer with high pressure sealing. Eng. Fail. Anal. 118, 104871. https://doi.org/10.1016/j.engfailanal.2020.104871.

Evers, R., Young, D.A., Vargus, G.W., et al., 2009. Design methodology for swellable elastomer packers in fracturing operations. In: Offshore Technology Conference. Houston, Texas, USA. https://doi.org/10.4043/20157-MS.

Hu, G., Zhang, P., Wang, G., et al., 2017. The influence of rubber material on sealing performance of packing element in compression packer. J. Nat. Gas Sci. Eng. 38, 120–138. https://doi.org/10.1016/j.jngse.2016.12.027.

Júnior, M.T., Zilio, G., Mortean, M.V.V., et al., 2023. Experimental and numerical analysis of transient thermal stresses on thick-walled cylinder. Int. J. Pres. Ves. Pip. 202, 104884. https://doi.org/10.1016/j.ijpvp.2023.104884.

Kim, B., Lee, S.B., Lee, J., et al., 2012. A comparison among Neo-Hookean model, Mooney-Rivlin model, and Ogden model for Chloroprene rubber. Int. J. Precis. Eng. Manuf. 13 (5), 759–764. https://doi.org/10.1007/s12541-012-0099-y.

Lan, W.J., Wang, H.X., Zhang, X., et al., 2019. Sealing properties and structure optimization of packer rubber under high pressure and high temperature. Petrol. Sci. 16 (3), 632–644. https://doi.org/10.1007/s12182-018-0296-0.

Liu, J., Dang, L., Fu, M., et al., 2014. Mechanical analysis of large deformation and double contact of packer rubber sleeve during axial compression. China Petrol. Mach. 42 (7), 49–54. 10. 3969/j. issn (in Chinese).

Liu, J., Deng, K., Liu, S., et al., 2021. Mechanical behavior and structure optimization of compressed PHP packer rubber. J. Mater. Eng. Perform. 30 (5), 3691–3704. https://doi.org/10.1007/s11665-021-05686-4.

Ma, W., Qu, B., Guan, F., 2014. Effect of the friction coefficient for contact pressure of packer rubber. Proceedings of the Institution of Mechanical Engineers, Part C: Journal of Mechanical Engineering Science 228 (16), 2881–2887. https://doi.org/10.1177/0954406214525596.

Melikoglu, M., 2014. Shale gas: analysis of its role in the global energy market. Renew. Sustain. Energy Rev. 37, 460–468. https://doi.org/10.1016/j.rser.2014.05.002.

Mooney, M., 1940. A theory of large elastic deformation. J. Appl. Phys. 11 (9), 582–592. https://doi.org/10.1063/1.1712836.

Ogden, R.W., 1972. Large deformation isotropic elasticity-On the correlation of theory and experiment for incompressible rubberlike solids. Proceedings of the Royal Society of London. Series A, Mathematical and Physical Sciences 326 (1567), 565–584. https://doi.org/10.1098/rspa.1972.0026.

Ogden, R.W., 1997. Nonlinear Elastic Deformations. Courier Corporation. https://doi.org/10.1115/1.3169137.

Patel, H., Salehi, S., Ahmed, R., et al., 2019a. Review of elastomer seal assemblies in oil & gas wells: performance evaluation, failure mechanisms, and gaps in industry standards. J. Petrol. Sci. Eng. 179, 1046–1062. https://doi.org/10.1016/j.petrol.2019.05.019.

Patel, H., Salehi, S., Teodoriu, C., et al., 2019b. Performance evaluation and parametric study of elastomer seal in conventional hanger assembly. J. Petrol. Sci. Eng. 175, 246–254. https://doi.org/10.1016/j.petrol.2018.12.051.

Rivlin, R.S., Saunders, D., 1997. Large elastic deformations of isotropic materials. In: Collected Papers of RS Rivlin. Springer, New York, NY, pp. 157–194. https://doi.org/10.1007/978-1-4612-2416-7_23.

Stephenson, M.H., 2016. Shale gas in North America and Europe. Energy Sci. Eng. 4 (1), 4–13. https://doi.org/10.1002/ese3.96.

Wang, H., Chen, S., Liu, Y., Zhang, L., et al., 2017. Numerical simulation and experimental validation for design improvement of packer rubber. Int. J. Simulat. Process Model. 12 (5), 419–428. https://doi.org/10.1504/IJSPM.2017.087603.

Yeoh, O.H., 1993. Some forms of the strain energy function for rubber. Rubber Chem. Technol. 66 (5), 754–771. https://doi.org/10.5254/1.3538343.

Zheng, X., Li, B., 2021. Study on sealing performance of packer rubber based on stress relaxation experiment. Eng. Fail. Anal. 129, 105692. https://doi.org/10.1016/j.engfailanal.2021.105692.

Zheng, C., Zheng, X., Qin, J., et al., 2021. Nonlinear finite element analysis on the sealing performance of rubber packer for hydraulic fracturing. J. Nat. Gas Sci. Eng. 85, 103711. https://doi.org/10.1016/j.jngse.2020.103711.

Zhang, F., Jiang, X., Wang, H., et al., 2018. Mechanical analysis of sealing performance for compression packer rubber tube. Mechanics and Industry 19, 309. https://doi.org/10.1051/meca/2017045.